

Ultraviolet Spectropolarimetry With Polstar: Using Polstar to test Magnetospheric Mass-loss Quenching

M. E. Shultz¹, R. Casini², M. C. M. Cheung³, A. David-Uraz^{4,5}, T. del Pino Alemán^{6,7}, C. Erba⁸, C. P. Folsom⁹, K. Gayley¹⁰, R. Ignace⁸, Z. Keszthelyi¹¹, O. Kochukhov¹², Y. Nazé¹³, C. Neiner¹⁴, M. Oksala¹⁵, V. Petit¹, P. A. Scowen¹⁶, N. Sudnik¹⁷, A. ud-Doula¹⁸, J. S. Vink¹⁹ and G. A. Wade^{20,21}

*Corresponding author(s). E-mail(s): mshultz@udel.edu;

Abstract

Polstar is a proposed NASA MIDEX space telescope that will provide high-resolution, simultaneous full-Stokes spectropolarimetry in the far ultraviolet, together with low-resolution linear polarimetry in the near ultraviolet. This observatory offers unprecedented capabilities to obtain unique information on the magnetic and plasma properties of the magnetospheres of hot stars. We describe an observing program making use of the known population of magnetic hot stars to test the fundamental hypothesis that magnetospheres should act to rapidly drain angular momentum, thereby spinning the star down, whilst simultaneously reducing the net mass-loss rate. Both effects are expected to lead to dramatic differences in the evolution of magnetic vs. non-magnetic stars.

Keywords: Ultraviolet astronomy (1736); Ultraviolet telescopes (1743); Space telescopes (1547); Circumstellar disks (235); Early-type emission stars (428); Stellar rotation (1629); Spectropolarimetry (1973); Polarimeters (1277); Instruments: Polstar; UV spectropolarimetry; NASA: MIDEX

1 Introduction

Stellar structure and evolution are both profoundly influenced by mass-loss and rotation. Mass-loss during the main sequence influences the pre-supernova mass of the star, as well as the mass of the remnant. Rapid rotation can lead to mixing in the convective core, replenishing the material available for nuclear fusion and thereby extending the main sequence lifetime. While few in number, massive stars dominate the mass and energy budgets of spiral galaxies, play a key role in regulating stellar ecologies by both quenching and triggering star formation, and are primary drivers of galactic chemical evolution, via their ionizing radiation, powerful stellar winds, supernova shockwaves, and internal nuclear furnaces.

Massive stars are also the progenitors of neutron stars and black holes, with the precise nature of the supernova remnant a given star leaves behind depending upon the details of its main sequence evolution. Understanding phenomena that modify mass-loss rates and stellar rotation at the top of the main sequence is therefore important in order to develop a comprehensive picture of the big picture processes that affect galactic structure, chemical composition, and the demographics of both main sequence and degenerate stars. Magnetic fields decisively alter both mass-loss and rotation, and therefore strongly affect stellar evolution.

Approximately 10% of stars with radiative envelopes possess magnetic fields, a fraction which is remarkably constant from spectral type A5 to

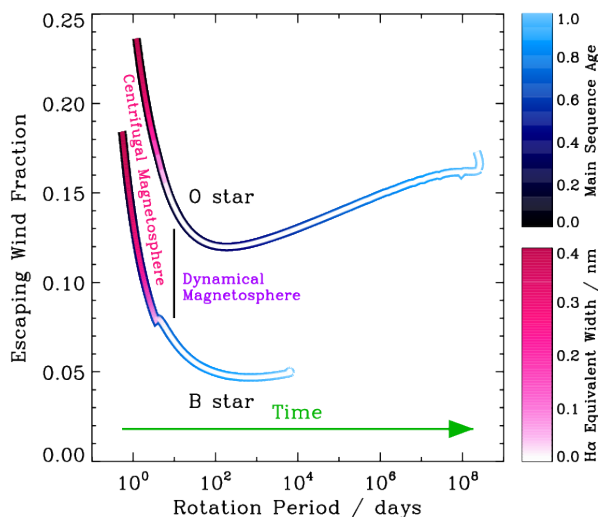


Fig. 1 MESA evolutionary models (Keszthelyi et al, 2020) showing the change in the escaping wind fraction as a function of the rotation period for an O- and B-type star, each with an initial magnetic field strength of 6 kG and an initial critical rotation fraction of 0.5. The H α equivalent width is calculated following an empirically guided centrifugal breakout formalism (Owocki et al, 2020; Shultz et al, 2020); note that centrifugal magnetospheres are only detectable via H α for the first third of the main sequence; in contrast, dynamical magnetospheres are detectable in the ultraviolet at all ages. The escaping wind fraction initially decreases as the centrifugal magnetosphere shrinks and centrifugal breakout declines in importance, and then begins to increase as the star’s increasing radius and luminosity drive an increased mass-loss rate, decreasing surface magnetic field strength (e.g. Shultz et al, 2019), and therefore the total size of the magnetosphere decreases.

the top of the main sequence (Grunhut et al, 2017; Schöller et al, 2017; Sikora et al, 2019). The magnetic fields of hot stars are in general strong (ranging from hundreds of G to tens of kG; Shultz et al, 2019), they are stable over timescales of at least decades (Shultz et al, 2018), and they are globally organized and, with few exceptions, geometrically simple (being well-described by tilted dipoles with most of the magnetic energy in low-order poloidal field components; Kochukhov et al, 2019). Stellar wind plasma can be trapped by a sufficiently strong magnetic field, leading to the formation of a circumstellar magnetosphere (e.g. ud-Doula and Owocki, 2002).

A detailed overview of the numerous multi-wavelength diagnostics available to probe magnetospheres, with a focus on the properties of ultraviolet diagnostics, together with the underlying physical models applied to stellar magnetospheres,

is provided in this volume by ud-Doula et al (2022). Briefly, hot star magnetospheres can be divided into two classes: dynamical and centrifugal (a taxonomy introduced by Petit et al, 2013). In a dynamical magnetosphere, rotation plays no role, and material trapped in the magnetosphere (i.e. material within the Alfvén surface) falls back to the star on dynamical timescales under the influence of gravity. In a centrifugal magnetosphere, corotation of the trapped plasma with the stellar magnetic field combines with rapid rotation to prevent infall of material above the Kepler corotation radius (e.g. Townsend and Owocki, 2005). Material trapped in the centrifugal magnetosphere is expected to build up to high density, before eventually being expelled away from the star by a form of magnetic reconnection referred to as ‘centrifugal breakout’ (ud-Doula et al, 2008), a phenomenon which has received observational support from the characteristic of both H α and radio gyrosynchrotron emission (e.g. Shultz et al, 2020; Owocki et al, 2020; Leto et al, 2021; Shultz et al, 2022; Owocki et al, 2022).

Since material trapped in a dynamical magnetosphere is returned to the star via gravitational infall, magnetic fields have the effect of reducing the net mass-loss rate¹ (ud-Doula and Owocki, 2002). Building on this phenomenon, Petit et al (2017) demonstrated that magnetospheric mass-loss quenching can reduce mass-loss rates by amounts comparable to a reduction of metallicity to that prevailing in the early, unenriched universe (since radiative winds are accelerated via line driving, mass-loss rates are a strong function of metallicity, e.g. Vink et al, 2001). Thus, magnetic stars are potential progenitors of the heavy stellar-mass black holes found by gravitational wave observations (Abbott et al, 2016; Petit et al, 2017), i.e. the formation of such objects is not limited to the early universe or to low-metallicity environments such as the Magellanic Clouds.

The second important consequence of a magnetosphere is to rapidly spin down a star (as revealed by MHD simulations conducted by ud-Doula et al, 2009). Evidence for spindown is seen in the extraordinarily long (\sim decades) rotational

¹It is important to note that stars with centrifugal magnetospheres still possess dynamical magnetospheres below the Kepler radius, and therefore still experience mass-loss quenching, except in the extreme case of critical rotation in which the Kepler radius is the same as the equatorial stellar radius

periods of some stars (e.g. Shultz and Wade, 2017; Shultz et al, 2017), the systematically lower projected rotational velocities of magnetic as compared to non-magnetic stars of similar spectral type (Shultz et al, 2018), and the systematic increase in rotational period with fractional main sequence age (Shultz et al, 2019).

Evolutionary models incorporating rotational spindown and mass-loss reduction have successfully reproduced the qualitative evolution of magnetic stars (e.g. Keszthelyi et al, 2019, 2020; Deal et al, 2021; Takahashi and Langer, 2021; Song et al, 2022), despite systematic uncertainty regarding factors such as the internal rotational profile. These models firmly predict that the evolutionary tracks of magnetic stars should differ considerably from those of stars without magnetic fields.

Keszthelyi et al (2020) demonstrated that the evolutionary tracks of magnetic stars with initially rapid rotation are markedly different from those of non-magnetic stars. The expected evolutionary scenario for magnetic hot stars – illustrated in Fig. 1 – is as follows: 1) young, rapid rotators with strong magnetic fields lose the majority of the trapped plasma from their CMs via centrifugal breakout (ud-Doula et al, 2008), during which period they evolve as stars with typical mass-loss rates and the usual effects of rapid rotation; 2) angular momentum loss quickly shrinks the CM, decreasing the net mass-loss rate as the DM grows from the inside out (ud-Doula et al, 2009), until; 3) the CM disappears, the DM slams shut on the wind, and the star evolves as an essentially non-rotating object with a nearly constant mass. As can be seen in Fig. 1, centrifugal magnetospheres disappear early in a magnetic star’s main sequence evolution, and become undetectable in H α at an even earlier phase (e.g. Shultz et al, 2019, 2020). In contrast, dynamical magnetospheres are detectable in the ultraviolet throughout a star’s evolution.

1.1 Polstar and motivation for this study

Polstar is a proposed NASA MIDEX space mission equipped with a 60-cm telescope and a full-Stokes (IQUV) spectropolarimeter divided in 2 channels in the ultraviolet (Scowen et al, 2021). The first channel provides spectropolarimetry at high

spectral resolution of $R \sim 33000$ over the 122-200 nm far-UV bandpass. The second channel provides spectropolarimetry over the 180-320 nm NUV band with low- to mid-resolution ($R \sim 30$ to 250). These wavelength ranges include particularly interesting resonance lines sensitive to the winds of hot stars, such as N v 123.9, 124.3 nm, Si iv 139.4, 140.3 nm, and C iv 154.8, 155.1 nm, as well as a large quantity of photospheric lines. Therefore Polstar is very well suited to study hot stars and their circumstellar environments.

High-resolution UV spectroscopy is relatively sparsely available for magnetic massive stars. A handful of objects have extensive time series, predominantly acquired with the International Ultraviolet Explorer (IUE) space telescope, with which the rotational modulation of their resonance lines can be examined; for other stars, only snapshot observations with IUE or the Hubble STIS or COS instruments are available, as the high time pressure on the HST makes it impractical to obtain high-cadence time series.

Even for stars with existing high-resolution UV spectroscopy, Channel 1 Polstar spectroscopy would provide several important advantages over existing data. First, the spectral resolution is higher than either IUE (about 8000) or HST/COS (about 15,000). Second, Polstar will be able to obtain a significantly higher signal-to-noise S/N : whereas a typical IUE spectrum has a $S/N \sim 10$, Polstar spectroscopy will easily reach values on the order of 100, and for some targets on the order of 1000. This will enable stellar rotation to be resolved in spectral lines, and will furthermore enable the detection of subtle features associated with magnetospheric activity.

While UV spectroscopy is available for some stars, UV spectropolarimetry and polarimetry is not. As described in detail by Folsom et al (2022) in this volume, these capabilities will enable Polstar data to detect and measure circumstellar magnetic fields, both in Stokes V via the Zeeman effect in wind-sensitive UV resonance lines, and via the Hanle effect in Stokes QU (which only works in the UV). Linear spectropolarimetry and broadband polarimetry will further offer unique information on the circumstellar geometry.

In the following, we describe how Polstar can be used to test the fundamental hypothesis that magnetic fields lead to angular momentum loss in the early part of a magnetic star’s evolution,

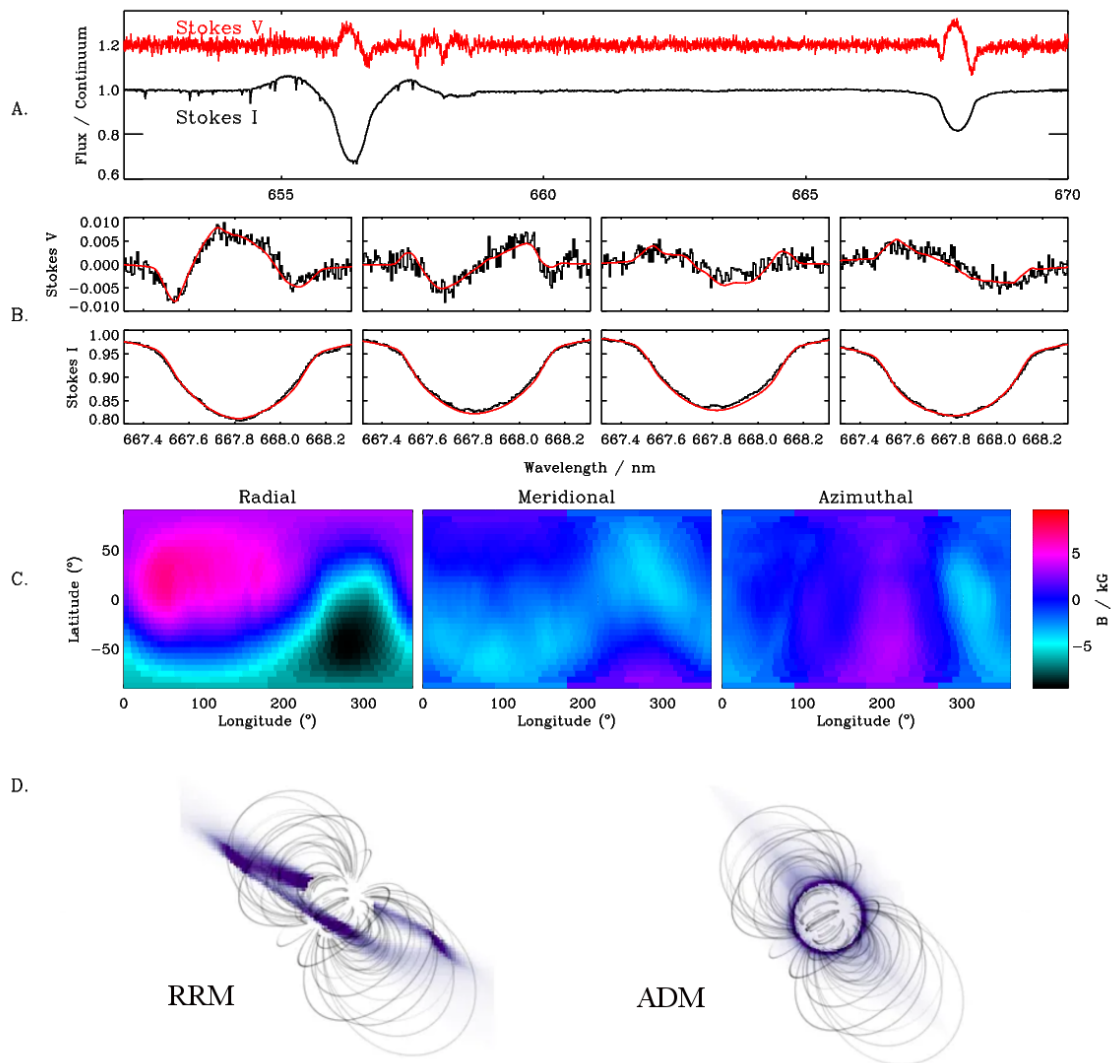


Fig. 2 Illustration of the data analysis flow. (A.) Polarized spectra of the target are acquired. (B.) Information from multiple rotational phases is combined in order to obtain (C.) a model of the surface magnetic field. Magnetospheric signatures (e.g. the H α line at 656 nm in (A.)) are then compared to predictions from (D.) Rigidly Rotating Magnetosphere (RRM) or Analytic Dynamical Magnetosphere (ADM) models obtained via extrapolation of the surface field into the circumstellar environment. The data and models shown in this figure are adapted from those presented by [Oksala et al \(2015\)](#) for σ Ori E (with the exception of the ADM model, which is based on the same field structure but has not previously been shown for this star).

while trapping material and dramatically reducing stellar mass-loss rates throughout the entirety of its main sequence lifetime. While the primary focus of this white paper pertains to the utility of Polstar to conduct such an experiment, the considerations developed here are of relevance to other proposed UV spectropolarimeters such as Arago ([Morin et al, 2019](#)), Pollux on LUVOIR ([Bouret](#)

[et al, 2018](#)), or any other similar mission that may be launched in the future.

2 Experimental design

The goal of observation of magnetic massive stars with Polstar is to test the theoretical prediction that magnetic confinement in the early, rapidly

Table 1 Summary of experimental design. From left to right, the columns give: the physical property of the target star being measured; the observational correlate of that property; the Polstar capability utilized; the requirements for the measurement to detect the feature of interest; the post-processing method used to reach the necessary signal-to-noise ratio; and the work in the present volume in which the relevant techniques are discussed with respect to Polstar.

Physical feature	Measurement	Mission Capability	Requirements	Method
Folsom et al., this volume				
Surface magnetic field	Zeeman effect in photospheric lines	Channel 1 Stokes IQUV	$R \sim 30,000$ pol. precision $\sim 10^{-4}$	LSD
Circumstellar magnetic field 1) $\gtrsim 100$ G 2) $\lesssim 100$ G	1) Zeeman effect in resonance lines 2) Hanle effect in resonance lines	1) Channel 1 Stokes IV 2) Channel 1 Stokes IQU	1) $R \sim 200 - 1500$ pol. precision $\sim 10^{-4}$ 2) $R \sim 200 - 1500$ pol. precision $\sim 10^{-4}$	1,2) Wavelength binning, co-addition of spectra
ud-Doula et al., this volume				
Magnetospheric velocity, column density	velocity-resolved flux in resonance lines	Channel 1 Stokes I	$R \sim 30,000$ $S/N \sim 100$	N/A
Magnetospheric geometry	1) scattering in resonance lines 2) scattering in continuum	1) Channel 1 Stokes IQU 2) Channel 2 Stokes QU	1) $R \sim 200 - 1500$, pol. precision $\sim 10^{-3}$ 2) pol. precision $\sim 10^{-5}$	1,2) Wavelength binning, co-addition of spectra

rotating evolutionary phase leads to rapid angular momentum loss accompanied by mass escape from the centrifugal magnetosphere via break-out, switching to a mass-trapping phase when the CM disappears and the magnetosphere locks down on the stellar wind, as illustrated in Fig. 1 (see also e.g. [ud-Doula et al, 2008, 2009](#)). This requires observation of magnetic hot stars across the full range of stellar parameters, evolutionary phases, rotational periods, and surface magnetic field strengths and geometries. Moreover, since magnetic wind confinement leads to rotational modulation of all signatures associated with the surface magnetic field, observations must be acquired sampling the full rotational phase curve – indeed, doing so enables magnetic and magnetospheric models to be inferred. Crucially, ultraviolet polarimetry will also enable the different components of the magnetosphere – the outflowing wind, and the trapped downflow – to be separately identified.

Uniquely amongst Polstar science objectives, the observation of magnetic stars will utilize the full range of the observatory’s capabilities: high-resolution spectroscopy, circular spectropolarimetry, linear spectropolarimetry, and broadband linear polarization. This comprehensive usage is summarized in Table 2. Each will provide key constraints that can be combined to obtain detailed

models of the three-dimensional density, velocity, and magnetic structure in the circumstellar environment, and linking this directly to the photospheric magnetic field and surface mass flux.

The initial steps of the analytic flow from observations to models is well illustrated by the case of the prototypical magnetosphere host star σ Ori E, for which a detailed magnetospheric analysis was performed by [Oksala et al \(2015\)](#). This flow is illustrated in Fig. 2.

1) Polarized spectra is obtained for a target. The S/N can be boosted with mean line profiles extracted via least-squares deconvolution (LSD; [Donati et al, 1997](#)). The surface magnetic field of the star is measured via the Zeeman effect.

2) Direct analysis of the Stokes V profiles enables detailed maps of the surface magnetic field via Zeeman Doppler Imaging (ZDI; [Piskunov and Kochukhov, 2002](#)).

3) The surface magnetic field is extrapolated into the circumstellar environment via potential field extrapolation. This is then used to guide Analytic Dynamical and Rigidly Rotating Magnetosphere models, providing predictions for the magnetospheric structure in the innermost region (where rotation is not important) and the outermost region (where rotation is key).

While steps 1) to 3) are possible with ground-based data, ultraviolet polarimetry will enable the following key steps:

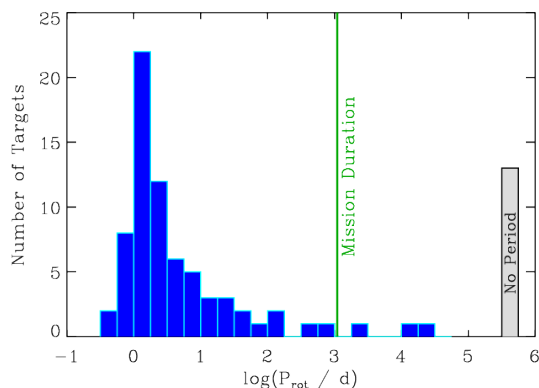


Fig. 3 Distribution of rotational periods for the sample. The green line indicates the approximate mission duration; complete phase coverage can be obtained for all stars below this limit, while the small number of stars with longer periods offer the opportunity to study intrinsic ultraviolet variability at nearly the same rotational phase.

- 4) Stokes V profiles in UV resonance lines will directly measure the circumstellar magnetic field, testing the expected decline in magnetic field strength with increasing distance from the star.
- 5) High-resolution spectroscopy and linear spectropolarimetry will provide information on the velocity and density structure in the magnetosphere and wind.
- 6) Broadband polarimetry will enable the magnetospheric geometry to be inferred via integrated light.

For each target, 10 high-resolution spectropolarimetric sequences will be obtained with Channel 1, and 30 low-resolution Channel 2 observations, with each dataset evenly sampling the rotational phase curve. The larger number of Channel 2 observations is necessitated by the complex behaviour of broadband linear polarimetry phase curves.

3 Sample description

The initial target list consists of those OB stars for which magnetic fields have been detected, comprising 84 stars in total, with most of the list having been drawn from the O-type stars listed by Petit et al (2013) and the B-type stars examined by Shultz et al (2018, 2019, 2020). For the majority of these stars, rotational periods are known (see Fig. 3) and magnetic oblique rotator

models are well characterized, with the 13 exceptions being either stars exhibiting no variability, or new discoveries for which sufficient followup data has not yet been obtained. Only 3 stars have periods longer than the 3-year mission duration; while rotational phase coverage cannot be completed for these targets, they are ideal for exploration of alternate science goals (e.g. examining intrinsic rather than rotationally modulated magnetospheric variability).

To evaluate the signal-to-noise ratio (S/N) that can be achieved for a given target, IUE spectra were acquired from the IUE archive. Where possible low-resolution spectra were utilized, as these more accurately preserve the true flux level than the high-resolution IUE data; otherwise high-resolution data were used. For each spectrum, the mean flux was calculated at 1500 Å and 2500 Å, as the approximate middle of the spectral ranges of Channels 1 and 2 respectively, with windows of ± 25 Å. When multiple spectra were available for a given target, the mean was calculated after discarding 3σ outliers.

Since IUE data are not available for all targets, synthetic spectra calculated using non-Local Thermodynamic Equilibrium (NLTE) TLUSTY models were also utilized in order to estimate the flux (Lanz and Hubeny, 2003, 2007). These were adjusted according to the radius of the star, the star's *Gaia* parallax distance, and the reddening inferred for the star's position on the sky and heliocentric distance using the tomographic STILISM three-dimensional tomographic dust map (Lallement et al, 2014; Capitanio et al, 2017). The left panel of Fig. 4 compares the IUE and TLUSTY fluxes, demonstrating a generally good agreement. The right panel shows histograms of the fluxes. When IUE fluxes are available, these are used; when not, we use TLUSTY fluxes.

Fig. 5 shows an important property of the sample that guides the observation strategy: there is a close relationship between F_{1500} and the measured values of the surface dipole strength B_d , such that the weakest fields are found in stars with the highest flux, whereas stars with lower flux have systematically stronger magnetic fields. This is a straightforward consequence of observational bias. Weak fields are intrinsically difficult to detect and therefore have only been measured in very bright targets. Conversely, the absence of

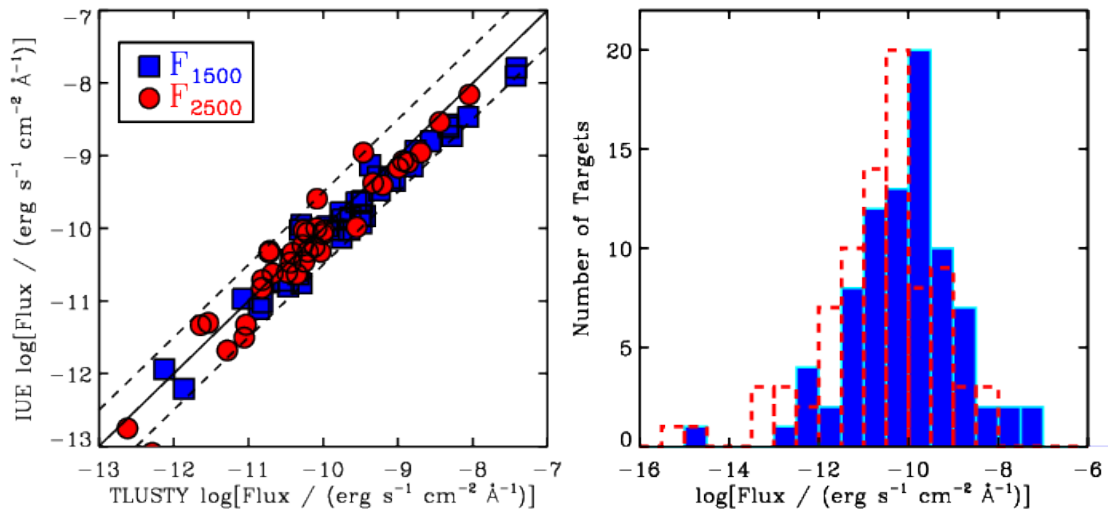


Fig. 4 *Left:* fluxes measured at 1500 Å and 2500 Å as a function of fluxes predicted from TLUSTY spectra; the solid and dashed lines show $x = y$ and the approximate scatter. *Right:* histograms for 1500 and 2500 Å fluxes for the full sample, combining both IUE fluxes (where available) and TLUSTY fluxes (where not).

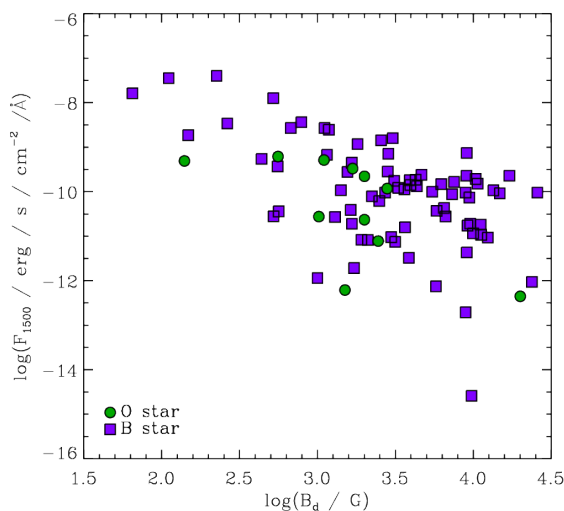


Fig. 5 Ultraviolet flux at 1500 Å F_{1500} as a function of surface dipole strength B_d . The weakest magnetic fields are preferentially found in brighter stars, due to observational bias.

very bright stars with extremely strong (~ 10 kG) magnetic fields is a result of their rarity. Since a stronger magnetic field can be measured with a lower S/N , rather than aiming for a uniform S/N , we adopt a uniform 1-hour exposure time, which as will be demonstrated below results in the detectability of circumstellar magnetic fields in the majority of the sample.

The S/N that can be achieved for a given target in a 3600 sec spectropolarimetric sequence was calculated according to:

$$S/N = \sqrt{\frac{\dot{S}_p^2 \Delta t^2}{\dot{S}_p \Delta t + 216 N_{\text{pix}} (\Delta t / 3600 \text{s}) + 175 N_{\text{pix}}}}, \quad (1)$$

where \dot{S}_p is the photon count rate, N_{pix} the number of pixels, and Δt is the total exposure time in seconds for all 6 sub-exposures. The second and third terms in the denominator of Eqn. 1 originate from the dark count rate and the read noise. $N_{\text{pix}} = 2 \times 2$ for Channel 1 and 2.5×2.5 for Channel 2. The photon count rate was estimated using

$$\dot{S}_p = \frac{f_\lambda}{g_\lambda}, \quad (2)$$

where f_λ is the flux at a given wavelength in units of $\text{erg s}^{-1} \text{cm}^{-2} \text{Å}^{-1}$ and g_λ is a factor with units of $\text{erg cm}^{-2} \text{Å}^{-1}$ given by

$$g_\lambda = \frac{R(\lambda)hc}{\lambda^2 A_{\text{eff}}(\lambda)}, \quad (3)$$

where R is spectral resolution, h and c are Planck's constant and the speed and light, and A_{eff} is the wavelength-dependent effective area.

The S/N that can be achieved using a 3600 s spectropolarimetric sequence in Channel 1 is shown in Fig. 6. The median S/N is 192. As

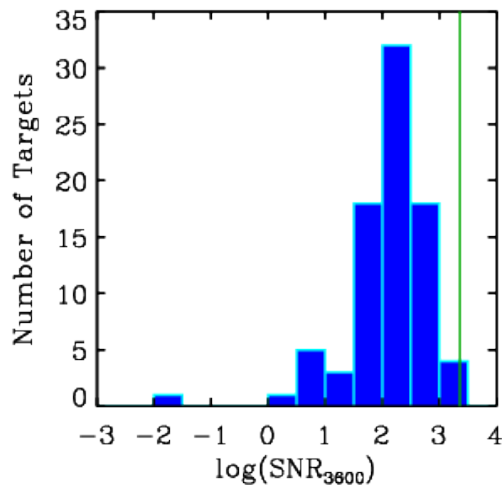


Fig. 6 S/N for a 3600 s Channel 1 spectropolarimetric sequence. The green line shows the saturation S/N .

explained below, we expect a S/N of 100 to be the approximate lower bound for surface magnetometry, while a S/N of 10 is sufficient for spectroscopy alone (this being a typical value for IUE spectra). Only 7 stars are below the spectroscopic threshold. If 10 3600 s observations are obtained for each of the 77 targets for which at least a S/N of 10 can be achieved, the total observing time necessary to complete Channel 1 coverage is 770 hours.

The detectability of the circumstellar magnetic fields threading the magnetosphere is demonstrated by Folsom et al (2022, , this volume), based on the Analytic Dynamical Magnetosphere (ADM; Owocki et al, 2016) model (see also ud-Doula et al, 2022, , this volume). ADM models simultaneously consider the free (magnetic unconfined) wind, the upflow feeding the magnetosphere, the stalled plasma within the magnetic equatorial plane, the downflowing plasma returning to the photosphere, and the wind shocks produced by collision of the upflow with the dense equatorial plasma. An extension of ADM incorporating radiative transfer was presented by Erba et al (2021) which enables synthesis of the unpolarized intensity profiles of wind-sensitive UV resonance lines. Since the ADM model naturally includes information on the local magnetic field strength and geometry in the circumstellar environment, a straightforward modification of the UV ADM model can also reproduce the circularly

polarized (Stokes V) profiles expected from the Zeeman effect. This is discussed in more detail by Folsom et al (2022, , this volume), and will be the subject of a dedicated work by Erba et al. (in prep.). The polarized UV ADM model provides predictions for both the amplitude and morphology of Stokes V as a function of magnetic field strength, wind parameters, and orientation with respect to the line of sight.

The ability of these measurements to detect circumstellar magnetic fields, as inferred from UV ADM Stokes V models is demonstrated in Fig. 7. Since B-type stars are expected to yield a larger Stokes V amplitude in resonance lines for a given field strength than O-type stars (see Folsom et al, 2022, , this volume), their circumstellar magnetic fields can be detected at a slightly lower S/N . Three of the most strongly magnetic B-type stars can be detected without wavelength binning. For the remainder of the sample, some degree of binning is necessary. The amount by which a given line can be binned is proportional to its line width. Taking the observed C IV doublets (ud-Doula et al, 2022, , this volume), B stars are expected to span about 1000 km s^{-1} , while O stars should span about 6000 km s^{-1} . In order to have a minimum of 5 measurements across the line, a B-type star can therefore adopt a maximum bin size of 200 km s^{-1} , while an O-star can be binned to a maximum of 1200 km s^{-1} . Such a strategy can detect circumstellar magnetic fields in 4 O-type stars and 32 B-type stars, or almost half the full sample. If each line in a resonance doublet can be co-added in order increase the S/N still further, in a process similar to LSD, the number of detectable B-stars increases to 44. Note that many of the B stars are detectable without applying this maximal degree of wavelength binning.

The right panel of Fig. 7 demonstrates the quality of the photospheric magnetometry that can be expected (see Folsom et al, 2022, , this volume), showing the 1500 \AA S/N as a function of the ratio of B_d to the error bar σ_B in $\langle B_z \rangle$. Since the maximum value of $\langle B_z \rangle$ is approximately $B_d/3.5$, a ratio of at least $\sigma_B/B_d = 0.1$ is ideal for the field to be securely detected and modelled. However, surface magnetic fields can often be detected with an error bar in $\langle B_z \rangle$ of about $1/3^{\text{rd}}$ of B_d , which we adopt as the magnetic limit. In this case, σ_B was determined using

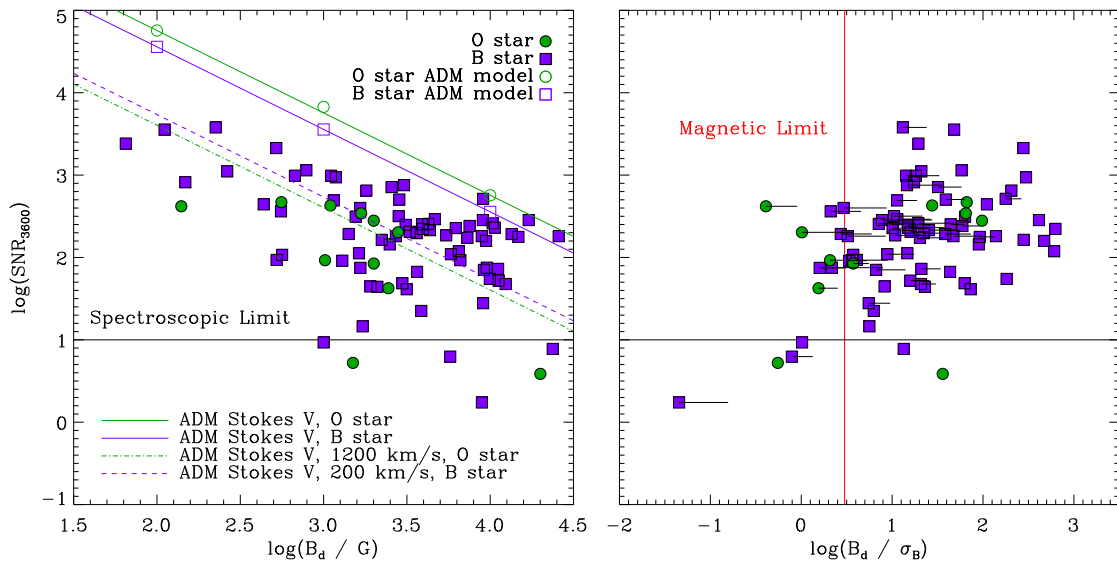


Fig. 7 *Left:* S/N for a 3600 s Channel 1 spectropolarimetric sequence as a function of B_d . Diagonal solid lines indicate the S/N required to detect a circumstellar magnetic field, as determined from ADM models for O and B-type stars. Diagonal dashed and dot-dashed lines indicate the S/N that can be achieved using bins of 200 km s⁻¹ and 1200 km s⁻¹, resulting in 5 wavelength bins across a resonance line for a B and an O-star, respectively. The solid horizontal line indicates the lower bound for useful spectroscopy. *Right:* S/N for a 3600 s Channel 1 spectropolarimetric sequence as a function of the ratio of B_d to the $\langle B_z \rangle$ error bar, where the error bar is inferred from UV LSD models and $v \sin i$. In order for the magnetic field to be measureable, the error bar must be about 1/3rd of B_d .

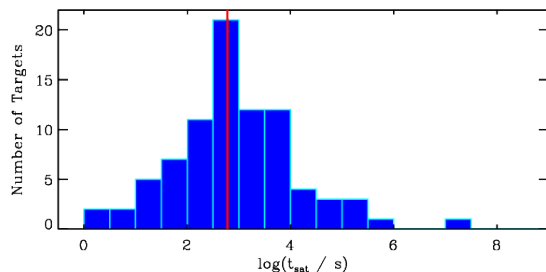


Fig. 8 Saturation time for Channel 2 observations. The red line shows the maximum observation 600 s length.

the $v \sin i$ and S/N -dependent relationships given by Wade et al (2016), with an LSD S/N gain inferred from the UV modelling (Folsom et al, 2022, , this volume). This figure demonstrates that the observations will be able to achieve the more challenging goal of surface magnetometry, as compared to the less challenging goal of spectroscopy, for all but 12 of the sample stars.

Channel 2 has a much larger effective area and a much lower spectral resolution than Channel 1, and therefore more easily reaches the saturation S/N of 2872. Fig. 8 shows the Channel 2 saturation times estimated using 2500 Å fluxes. The

median saturation time is 775 s. Two stars reach saturation time in less than the minimum sub-exposure time of 2 s, and therefore cannot be observed in Channel 2. There are 38 observable stars which reach saturation time in less than 600 s. If the Channel 2 dataset is limited to these stars, and 30 observations are obtained for each target in order to obtain the necessary dense coverage of the QU plane, completing this component of the observing program will require 76 hours.

As discussed by ud-Doula et al (2022, , this volume), the expected level of continuum polarization, as inferred from observations using visible data, ranges from on the order of 0.01% to 0.1%. Taking the lower bound, this implies that a S/N of at least 10,000 is necessary to obtain a precision sufficient to obtain a 5σ measurement of the weakest expected signals. This can be easily achieved by wavelength binning: while Channel 2 has a low spectral resolution, the required high S/N is easily achievable by binning around 10 wavelength elements.

Fig. 9 shows a histogram of the number of high-resolution UV observations available for the target stars. There are no data available for 28 stars. For

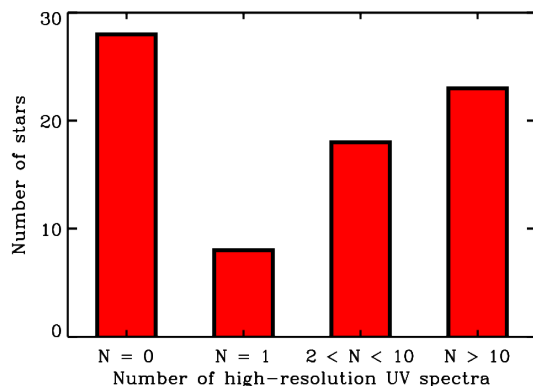


Fig. 9 Histogram summary of the available high-resolution UV spectroscopy. The sample is about evenly divided into stars with no observations, stars with a large number of observations, and stars with only a few observations.

8 stars, only a single snapshot is available, therefore variability cannot be assessed. Between 2 and 10 observations are available for 18 stars; in these cases, some limited evaluation of variability is possible, but coverage of the rotational period is poor. For 23 stars more than 10 observations are available; in these cases detailed studies have generally been possible (e.g. [Neiner et al, 2003a,b](#); [Henrichs et al, 2013](#)). A key program goal is to obtain sufficient observations to characterize the ultraviolet variability across the full rotational period of the entire sample. A particular point of interest is the red-shifted absorption dip identified by ADM models ([ud-Doula et al., this volume](#); see also [Erba et al, 2021](#)), which is diagnostic of the infalling plasma. Detecting this feature will require both a high spectral resolution (as it has an expected velocity width of about 100 km s^{-1}), and high S/N .

The left panel of Fig. 10 shows the full sample on the rotation-magnetic confinement diagram, the ‘fundamental plane’ of stellar magnetospheres ([Petit et al, 2013](#)). This diagram shows the Kepler corotation radius R_K as a function of the Alfvén radius R_A . As a star rotates more rapidly, R_K withdraws towards the stellar surface, becoming identical with the equatorial radius of the star at critical rotation. The Alfvén radius is a measure of the extent of magnetic confinement in the magnetic equatorial plane, and increases with increasing surface magnetic field and declining wind strength. As a star rotates more rapidly,

the Kepler radius moves closer to the stellar surface. The right panel of Fig. 10 shows the sample stars on the $\log R_A/R_K - \log L_{\text{bol}}$ diagram. The ratio $\log R_A/R_K$ serves as a dimensionless proxy to the size of the CM. As can be seen in these diagrams, the majority of the O-type stars have dynamical magnetospheres, as they have powerful winds leading to small R_A and rapid spindown timescales, meaning slow rotation and therefore large R_K . Conversely, the majority of B-type stars have centrifugal magnetospheres.

As indicated in Fig. 10, while at least one UV observation is available for all magnetic O-type stars, a considerable fraction of magnetic B-type stars have not been observed in the UV. Variable UV emission are seen at essentially all points in the two diagrams, raising the obvious question of why some stars that have been observed do not show obvious magnetospheric signatures (coded in the diagram as UV absorption). As suggested by the symbol size (proportional to the number of spectra), this may simply be the result of a small number of observations, which make it difficult or impossible to evaluate variability in the wind-sensitive doublets.

3.1 Threshold Targets

A subset of the sample were selected as *threshold targets*, i.e. high-priority targets. The first criterion regarding these targets is that they be bright enough for Polstar to obtain a high signal-to-noise ratio (S/N). Beyond this, it is important to sample parameter space whilst also observing the most interesting targets. As can be seen in Fig. 10, the critical targets were chosen in such a fashion as to cover the various key parts of parameter space: B stars with large CMs, B stars with DMs, O stars with CMs, and O stars with DMs. The threshold targets are:

θ^1 Ori C: HD 37022 is the most massive O-type star in the Orion Nebula Cluster and was the first O-type star in which a magnetic field was discovered ([Donati et al, 2002](#)). It exhibits phase-locked ultraviolet variability consistent with a magnetospheric origin ([Stahl et al, 1996](#)), although the observed variability is contrary to expectations, being anti-correlated in phase ([ud-Doula, 2008](#)). This points to an important discrepancy between models and observations, which may be

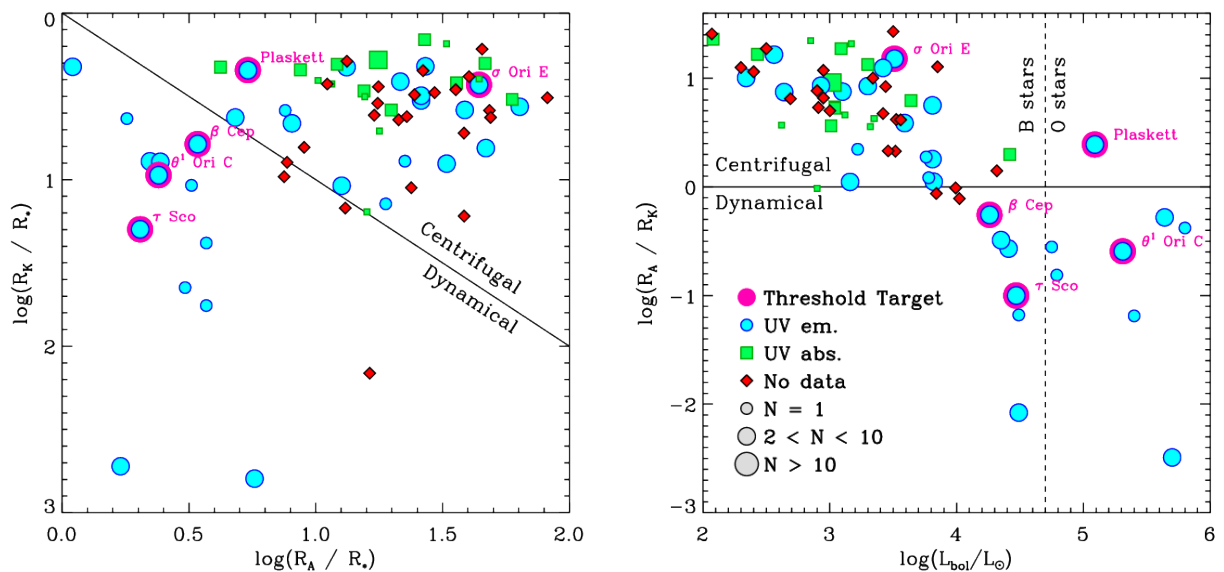


Fig. 10 *Left:* survey sample on the rotation-magnetic confinement diagram. As indicated by the slanted line, stars with Alfvén radii R_A greater than Kepler corotation radii R_K have centrifugal magnetospheres, while those with $R_A < R_K$ have dynamical magnetospheres. Symbol size is proportional to the number of available high-resolution UV spectra. Colour indicates whether magnetospheric emission is detected, not detected, or if no data are available. Threshold targets are highlighted in magenta and labelled. *Right:* as left, in the bolometric luminosity- $\log R_A/R_K$ plane.

resolved by the structural and magnetic information obtained via circumstellar polarimetry.

σ Ori E: HD 37479 was the first star in which a magnetosphere was detected (Landstreet and Borra, 1978) and is the prototype of the σ Ori E variable class (i.e. stars with H α emission and photometric eclipses from a CM). It has by far the strongest magnetospheric emission of any CM star (Shultz et al, 2020). It has a large IUE dataset (e.g. Smith and Groote, 2001), and as the benchmark CM star has also been extensively studied at radio and X-ray wavelengths (e.g. Reiners et al, 2000; Leto et al, 2012). Furthermore, its surface magnetic field has been mapped via Zeeman Doppler Imaging, and a magnetospheric model extrapolated from this map used to reproduce its H α emission and photometric eclipses (Oksala et al, 2015). It is also the only CM star with published broadband polarimetry (Carciofi et al, 2013). Adding Polstar spectropolarimetry to the large multiwavelength datasets and extensive modeling already performed for this star will be a key step in calibrating the next generation of magnetospheric models that will be enabled by Polstar.

Plaskett’s Star: HD 47129 is a magnetic colliding wind binary historically considered to consist of two O-type stars, one of which is the only O-type star with a CM (Grunhut et al, 2013, 2021). The star’s rapid rotation is believed to be a result of recent binary interactions. Polstar data will enable evaluation of the effects of rapid rotation on the circumstellar environment in an O-type star’s magnetosphere, together with examination of the effects of a strong magnetic field on the colliding wind shock.

τ Sco: HD 149438 is the hottest B-type star with a detected magnetic field, and in sharp contrast to the usual dipolar morphology has an extraordinarily complex surface field structure (Donati et al, 2006; Kochukhov and Wade, 2016). Its distinctive ultraviolet resonance line profiles were the crucial clue leading to the detection of its magnetic field (Donati et al, 2006); similar ultraviolet signatures have successfully enabled the identification of other magnetic stars in the same mass range (Petit et al, 2011). It has been suggested to be a blue straggler and a possible binary merger product, with its complex surface field being the remnant of a merger-powered dynamo (Schneider et al, 2019), although its properties may also

be consistent with single-star evolutionary models incorporating magnetic fields (Keszthelyi et al, 2021). As the surface magnetic field of this bright star is relatively weak, it is an excellent target for utilization of the Hanle effect.

β Cep: HD 205021 is a magnetic β Cep pulsator. It features by far the largest IUE time series of any magnetic star, and exhibits clear and strong rotational modulation in all wind-sensitive resonance lines; indeed, it was precisely this modulation that led to the detection of its magnetic field (Henrichs et al, 2013), with comparable ultraviolet signatures in other β Cep stars leading to the detection of further magnetic stars in this class (Schnerr et al, 2008; Shultz et al, 2017). While this star is a spectroscopic binary with a Be companion star that contributes H α emission, the companion is otherwise undetectable in visible light aside from radial velocity variations and will therefore certainly be almost undetectable at UV wavelengths (Henrichs et al, 2013).

4 Synergies with other science objectives

Hot star winds: Gayley et al (2021) describe the utility of Polstar for calibrating the mass-loss rates of hot stars via their radiative winds in light of wind structures such as clumping and the corotating interaction regions (CIRs) thought to underlie discrete absorption components (DACs). The calibrated mass-loss rates obtained via this project for single stars without large-scale magnetic fields will inform the surface mass-flux for magnetospheric models described here. This will enable it to be determined whether strong surface magnetic fields directly modify the surface mass-flux via radiative winds. In addition, CIRs are thought to be driven by bright spots, which are believed to be associated with small-scale magnetic fields. Magnetospheric models developed from the study of magnetic hot stars may prove to be an important component of modelling CIRs. Weak magnetic fields in the launch regions of CIRs may also be detectable via the Hanle effect.

The origin of rapidly rotating B-type stars: Jones et al (2021) will use Polstar to search for hot subdwarf companions around apparently single classical Be stars and Bn stars, for which binary interactions are a leading origin scenario

for the spin-up of Be stars to near-critical rotation. Binary mergers are a leading scenario for the origin of fossil magnetic fields, presenting an intriguing dichotomy in that no magnetic field has ever been detected in a Be star, and indeed magnetic fields should destroy their Keplerian disks. Techniques developed from binary searches for subdwarf companions around Be/n stars can be applied to magnetic hot stars in a similar fashion, enabling sensitive comparison of their respective binary fractions; at this point, it is already known that most, albeit not all, magnetic stars are apparently single, whereas Be stars when in binary systems are typically paired with post-main sequence companions). Jones et al also describe the use of limb polarization to determine the critical rotation fraction of rapid rotators. While most magnetic stars are relatively slowly rotating, there are a handful of relatively rapidly rotating objects for which similar techniques will provide important constraints. Since the surface mass flux is sensitive to the effective temperature, gravity darkening due to rapid rotation may need to be incorporated in magnetospheric models of rapidly rotating objects. Finally, while magnetic fields are neither detected nor expected in Be/n stars, the Hanle effect may enable detection of weak magnetic fields in the near-star environment if present, and sensitive upper limits if not.

Mass transfer and loss in B-type interacting binaries: Peters et al (2021) describe Polstar's application to interacting binary systems, which can be used to constrain the geometry, mass transfer, and mass loss rates of interaction regions and circumbinary disks in interacting binaries. While magnetic binaries are rare, there are a handful of systems (e.g. ϵ Lupi, HD 149277) which are close enough for wind interactions to play a role, and which therefore hold the promise of determining whether and to what degree surface magnetic fields modify these interactions.

Massive star binary colliding winds: St-Louis et al (2021) describe the utility of Polstar to constrain the geometry of colliding wind binaries. Weak magnetic fields are required to reproduce the gyrosynchrotron radiation detected from colliding wind binaries; while these magnetic fields are too weak to be detected via the Zeeman effect, they may be detectable via the Hanle effect. Furthermore, the rapidly rotating magnetic O-type system Plaskett's Star is a colliding wind

binary; a complete understanding of the circumstellar geometry of this system is almost certain to require insights obtained from the study of magnetic stars and non-magnetic colliding wind binaries.

Interstellar medium science: [Andersson et al \(2021\)](#) describe several experiments that will investigate the dust polarization properties of the interstellar medium (ISM). Constraints from the ISM project will be a critical element for interpretation of the linear polarization signatures obtained from magnetic stars. Conversely, detailed understanding of the variable intrinsic polarization of magnetic stars will enable these targets to be added to the ISM project.

Protoplanetary disks: [Wisniewski et al \(2021\)](#) describe the use of Polstar to probe the circumstellar geometry of the protoplanetary disks surrounding Herbig Ae/Be stars in order to determine the nature of the accretion mechanism. Accretion is believed to be magnetospheric in low-mass Herbig stars, but the mechanism unknown for stars more massive than $4 M_{\odot}$. Comparing accretion signatures of Herbig stars with and without magnetic fields may furthermore provide important insights into the origin of fossil fields, and the reason for the magnetic dichotomy between main sequence stars with and without magnetic fields.

5 Summary

In this paper we have described how the unique capabilities offered by Polstar will lead to fundamental advances in our understanding of the magnetospheres of hot stars. While the focus of this white paper has been on the capabilities of the Polstar mission, this work is of relevance to any ultraviolet spectropolarimetric mission, such as e.g. Arago.

The high-resolution ultraviolet spectra obtained by Polstar will enable much more precise spectroscopic evaluation of stellar magnetospheres, as compared to the lower-resolution, lower- S/N data available for most stars via the Interstellar Ultraviolet Explorer. Importantly, over half of the none magnetic stars have not a single UV observation; of those that do, less than a third have time-series data adequate for evaluation of the projected magnetospheric geometry and column density across a rotational cycle.

While surface magnetic field measurements obtained via ground-based visible spectropolarimetry are already available for all stars in the sample, the large number of spectral lines available for multi-line analysis in high-resolution ultraviolet spectra more than compensates for the weaker Zeeman effect at shorter wavelengths, in principle enabling higher-precision magnetic measurements to be obtained in the UV as compared to the visible. The full-Stokes capability of Polstar, and expected advantages in the UV over the visible in the amplitude of Stokes QU signals associated with the transverse Zeeman effect, mean that many of the datasets will be optimal for magnetic mapping via full-Stokes Zeeman Doppler Imaging. Importantly, the availability of all four Stokes parameters for magnetic inversion breaks degeneracies that can affect maps obtained only in Stokes IV .

Polstar will enable measurement of circumstellar magnetic fields, with the projected capabilities of the instrument capable of detecting magnetic signatures originating in the circumstellar environment in a large fraction of known magnetic stars. Strong fields should be detectable via the Zeeman effect (as evaluated using state of the art magnetospheric models), while weak magnetic fields should be detectable via the Hanle effect.

Both high- and low- resolution linear spectropolarimetry will provide crucial and sensitive constraints on the magnetospheric geometry, enabling degeneracies between rotational axis inclinations and magnetic axis tilt angles to be broken. Importantly, the information available via linear polarization provides geometrical data that cannot be obtained via spectroscopy or photometry alone, as already revealed by the insufficiency of current magnetospheric models to simultaneously reproduce the light curve and polarimetric variation of the key target σ Ori E.

By combining the rich spectroscopic and polarimetric datasets available with Polstar observations, detailed 3D models of the circumstellar environments of a large number of magnetic hot stars can be compared against constraints on the circumstellar magnetic field, column density, velocity structure, and geometry. This will enable measurement of the escaping and magnetically trapped wind fraction of these stars across a full range of stellar, evolutionary, magnetic, and rotational parameters, thereby providing a crucial test

of the expectation that magnetic fields rapidly drain angular momentum and drastically reduce the net mass-loss rates of massive stars. This will provide empirical calibration for evolutionary models incorporating rotation and magnetic fields, which will in turn provide important information for the stellar population synthesis models used to infer the mass and energy budget for the interstellar medium, expectations for the properties of post-main sequence supergiants and supernovae, and the population statistics of stellar remnants.

References

- Abbott BP, Abbott R, Abbott TD, et al (2016) Observation of Gravitational Waves from a Binary Black Hole Merger. *PhysRevLett*116(6):061102. <https://doi.org/10.1103/PhysRevLett.116.061102>, <https://arxiv.org/abs/arXiv:1602.03837> [gr-qc]
- Andersson BG, Clayton GC, Doney KD, et al (2021) Ultraviolet Spectropolarimetry with Polstar: Interstellar Medium Science. arXiv e-prints arXiv:2111.08079. <https://arxiv.org/abs/arXiv:2111.08079> [astro-ph.GA]
- Bouret JC, Neiner C, Gómez de Castro AI, et al (2018) The science case for POLLUX: a high-resolution UV spectropolarimeter onboard LUVOIR. In: den Herder JWA, Nikzad S, Nakazawa K (eds) *Space Telescopes and Instrumentation 2018: Ultraviolet to Gamma Ray*, p 106993B, <https://doi.org/10.1117/12.2312621.1805.10021>
- Capitanio L, Lallement R, Vergely JL, et al (2017) Three-dimensional mapping of the local interstellar medium with composite data. *A&A*606:A65. <https://doi.org/10.1051/0004-6361/201730831>, <https://arxiv.org/abs/arXiv:1706.07711> [astro-ph.GA]
- Carciofi AC, Faes DM, Townsend RHD, et al (2013) Polarimetric Observations of σ Orionis E. *ApJL*766(1):L9. <https://doi.org/10.1088/2041-8205/766/1/L9>, <https://arxiv.org/abs/arXiv:1302.4684> [astro-ph.SR]
- Deal M, Cunha MS, Keszthelyi Z, et al (2021) Fundamental properties of a selected sample of Ap stars: Inferences from interferometric and asteroseismic constraints. *A&A*650:A125. <https://doi.org/10.1051/0004-6361/202040234>, <https://arxiv.org/abs/arXiv:2104.08097> [astro-ph.SR]
- Donati JF, Semel M, Carter BD, et al (1997) Spectropolarimetric observations of active stars. *MNRAS*291(4):658–682. <https://doi.org/10.1093/mnras/291.4.658>
- Donati JF, Babel J, Harries TJ, et al (2002) The magnetic field and wind confinement of θ^1 Orionis C. *MNRAS*333(1):55–70. <https://doi.org/10.1046/j.1365-8711.2002.05379.x>
- Donati JF, Howarth ID, Jardine MM, et al (2006) The surprising magnetic topology of τ Sco: fossil remnant or dynamo output? *MNRAS*370(2):629–644. <https://doi.org/10.1111/j.1365-2966.2006.10558.x>, <https://arxiv.org/abs/arXiv:astro-ph/0606156> [astro-ph]
- Erba C, David-Uraz A, Petit V, et al (2021) Ultraviolet line profiles of slowly rotating massive star winds using the ‘analytic dynamical magnetosphere’ formalism. *MNRAS*506(4):5373–5388. <https://doi.org/10.1093/mnras/stab1853>, <https://arxiv.org/abs/arXiv:2106.13676> [astro-ph.SR]
- Folsom CP, Ignace R, Erba C, et al (2022) Ultraviolet Spectropolarimetry: Investigating stellar magnetic field diagnostics. arXiv e-prints arXiv:2207.01865. <https://arxiv.org/abs/arXiv:2207.01865> [astro-ph.SR]
- Gayley K, Vink JS, ud-Doula A, et al (2021) Ultraviolet Spectropolarimetry with Polstar: Clumping and Mass-loss Rate Corrections. arXiv e-prints arXiv:2111.11633. <https://arxiv.org/abs/arXiv:2111.11633> [astro-ph.SR]
- Grunhut JH, Wade GA, Leutenegger M, et al (2013) Discovery of a magnetic field in the rapidly rotating O-type secondary of the colliding-wind binary HD

- 47129 (Plaskett's star). *MNRAS*428:1686–1695. <https://doi.org/10.1093/mnras/sts153>, <https://arxiv.org/abs/arXiv:1209.6326> [astro-ph.SR]
- Grunhut JH, Wade GA, Neiner C, et al (2017) The MiMeS survey of Magnetism in Massive Stars: magnetic analysis of the O-type stars. *MNRAS*465:2432–2470. <https://doi.org/10.1093/mnras/stw2743>, <https://arxiv.org/abs/arXiv:1610.07895> [astro-ph.SR]
- Grunhut JH, Wade GA, Folsom CP, et al (2021) The magnetic field and magnetosphere of Plaskett's star: A fundamental shift in our understanding of the system. arXiv e-prints arXiv:2111.06251. <https://arxiv.org/abs/arXiv:2111.06251> [astro-ph.SR]
- Henrichs HF, de Jong JA, Verdugo E, et al (2013) Discovery of the magnetic field in the pulsating B star β Cephei. *A&A*555:A46. <https://doi.org/10.1051/0004-6361/201321584>, <https://arxiv.org/abs/arXiv:1305.2601> [astro-ph.SR]
- Jones CE, Labadie-Bartz J, Nazé Y, et al (2021) Ultraviolet Spectropolarimetry with Polstar: on the origin of rapidly rotating B stars. arXiv e-prints arXiv:2111.07926. <https://arxiv.org/abs/arXiv:2111.07926> [astro-ph.IM]
- Keszthelyi Z, Meynet G, Georgy C, et al (2019) The effects of surface fossil magnetic fields on massive star evolution: I. Magnetic field evolution, mass-loss quenching, and magnetic braking. *MNRAS*485(4):5843–5860. <https://doi.org/10.1093/mnras/stz772>, <https://arxiv.org/abs/arXiv:1902.09333> [astro-ph.SR]
- Keszthelyi Z, Meynet G, Shultz ME, et al (2020) The effects of surface fossil magnetic fields on massive star evolution - II. Implementation of magnetic braking in MESA and implications for the evolution of surface rotation in OB stars. *MNRAS*493(1):518–535. <https://doi.org/10.1093/mnras/staa237>, <https://arxiv.org/abs/arXiv:2001.06239> [astro-ph.SR]
- Keszthelyi Z, Meynet G, Martins F, et al (2021) The effects of surface fossil magnetic fields on massive star evolution - III. The case of τ Sco. *MNRAS*504(2):2474–2492. <https://doi.org/10.1093/mnras/stab893>, <https://arxiv.org/abs/arXiv:2103.13465> [astro-ph.SR]
- Kochukhov O, Wade GA (2016) Magnetic field topology of τ Scorpii. The uniqueness problem of Stokes V ZDI inversions. *A&A*586:A30. <https://doi.org/10.1051/0004-6361/201527454>, <https://arxiv.org/abs/arXiv:1511.07881> [astro-ph.SR]
- Kochukhov O, Shultz M, Neiner C (2019) Magnetic field topologies of the bright, weak-field Ap stars θ Aurigae and ϵ Ursae Majoris. *A&A*621:A47. <https://doi.org/10.1051/0004-6361/201834279>, <https://arxiv.org/abs/arXiv:1811.04928> [astro-ph.SR]
- Lallement R, Vergely JL, Valette B, et al (2014) 3D maps of the local ISM from inversion of individual color excess measurements. *A&A*561:A91. <https://doi.org/10.1051/0004-6361/201322032>, <https://arxiv.org/abs/arXiv:1309.6100> [astro-ph.GA]
- Landstreet JD, Borra EF (1978) The magnetic field of Sigma Orionis E. *ApJL*224:L5–L8. <https://doi.org/10.1086/182746>
- Lanz T, Hubeny I (2003) A Grid of Non-LTE Line-blanketed Model Atmospheres of O-Type Stars. *ApJS*146(2):417–441. <https://doi.org/10.1086/374373>, <https://arxiv.org/abs/arXiv:astro-ph/0210157> [astro-ph]
- Lanz T, Hubeny I (2007) A Grid of NLTE Line-blanketed Model Atmospheres of Early B-Type Stars. *ApJS*169(1):83–104. <https://doi.org/10.1086/511270>, <https://arxiv.org/abs/arXiv:astro-ph/0611891> [astro-ph]

- Leto P, Trigilio C, Buemi CS, et al (2012) Searching for a CU Virginis-type cyclotron maser from σ Orionis E: the role of the magnetic quadrupole component. *MNRAS* 423:1766–1774. <https://doi.org/10.1111/j.1365-2966.2012.20997.x>, <https://arxiv.org/abs/arXiv:1203.6475> [astro-ph.SR]
- Leto P, Trigilio C, Krtićka J, et al (2021) A scaling relationship for non-thermal radio emission from ordered magnetospheres: from the top of the main sequence to planets. *MNRAS* 507(2):1979–1998. <https://doi.org/10.1093/mnras/stab2168>, <https://arxiv.org/abs/arXiv:2107.11995> [astro-ph.SR]
- Morin J, Bouret JC, Neiner C, et al (2019) Stellar Physics with High-Resolution UV Spectropolarimetry. arXiv e-prints arXiv:1908.01545. <https://arxiv.org/abs/arXiv:1908.01545> [astro-ph.SR]
- Neiner C, Geers VC, Henrichs HF, et al (2003a) Discovery of a magnetic field in the Slowly Pulsating B star ι ASTROBJ_{zeta} Cassiopeiae/ ι ASTROBJ_{zeta}. *A&A* 406:1019–1031. <https://doi.org/10.1051/0004-6361:20030742>
- Neiner C, Henrichs HF, Floquet M, et al (2003b) Rotation, pulsations and magnetic field in ι ASTROBJ_V 2052 Ophiuchi/ ι ASTROBJ_{zeta}: A new He-strong star. *A&A* 411:565–579. <https://doi.org/10.1051/0004-6361:20031342>
- Oksala ME, Kochukhov O, Krtićka J, et al (2015) Revisiting the rigidly rotating magnetosphere model for σ Ori E - II. Magnetic Doppler imaging, arbitrary field RRM, and light variability. *MNRAS* 451(2):2015–2029. <https://doi.org/10.1093/mnras/stv1086>, <https://arxiv.org/abs/arXiv:1505.04839> [astro-ph.SR]
- Owocki SP, ud-Doula A, Sundqvist JO, et al (2016) An ‘analytic dynamical magnetosphere’ formalism for X-ray and optical emission from slowly rotating magnetic massive stars. *MNRAS* 462(4):3830–3844. <https://doi.org/10.1093/mnras/stw1894>, <https://arxiv.org/abs/arXiv:1607.08568> [astro-ph.SR]
- Owocki SP, Shultz ME, ud-Doula A, et al (2020) How the breakout-limited mass in B-star centrifugal magnetospheres controls their circumstellar H α emission. *MNRAS* 499(4):5366–5378. <https://doi.org/10.1093/mnras/staa2325>, <https://arxiv.org/abs/arXiv:2009.12359> [astro-ph.SR]
- Owocki SP, Shultz ME, ud-Doula A, et al (2022) Centrifugal breakout reconnection as the electron acceleration mechanism powering the radio magnetospheres of early-type stars. arXiv e-prints arXiv:2202.05449. <https://arxiv.org/abs/arXiv:2202.05449> [astro-ph.SR]
- Peters GJ, Gayley K, Ignace R, et al (2021) Ultraviolet Spectropolarimetry with Polstar: Conservative and Nonconservative Mass Transfer in OB Interacting Binaries. arXiv e-prints arXiv:2111.14047. <https://arxiv.org/abs/arXiv:2111.14047> [astro-ph.SR]
- Petit V, Massa DL, Marcolino WLF, et al (2011) Discovery of the first τ Sco analogues: HD 66665 and HD 63425. *MNRAS* 412:L45–L49. <https://doi.org/10.1111/j.1745-3933.2010.01002.x>, <https://arxiv.org/abs/arXiv:1012.4445> [astro-ph.SR]
- Petit V, Owocki SP, Wade GA, et al (2013) **P13:** A magnetic confinement versus rotation classification of massive-star magnetospheres. *MNRAS* 429:398–422. <https://doi.org/10.1093/mnras/sts344>, <https://arxiv.org/abs/arXiv:1211.0282> [astro-ph.SR]
- Petit V, Keszthelyi Z, MacInnis R, et al (2017) Magnetic massive stars as progenitors of ‘heavy’ stellar-mass black holes. *MNRAS* 466(1):1052–1060. <https://doi.org/10.1093/mnras/stw3126>, <https://arxiv.org/abs/arXiv:1611.08964> [astro-ph.SR]
- Piskunov N, Kochukhov O (2002) Doppler Imaging of stellar magnetic fields. I. Techniques. *A&A* 381:736–756. <https://doi.org/10.1051/0004-6361:20011517>
- Reiners A, Stahl O, Wolf B, et al (2000) Modeling

- line profile variations of sigma Ori E and theta¹ Ori C. *A&A*363:585–592
- Schneider FRN, Ohlmann ST, Podsiadlowski P, et al (2019) Stellar mergers as the origin of magnetic massive stars. *Nature*574(7777):211–214. <https://doi.org/10.1038/s41586-019-1621-5>, <https://arxiv.org/abs/arXiv:1910.14058> [astro-ph.SR]
- Schnerr RS, Henrichs HF, Neiner C, et al (2008) Magnetic field measurements and wind-line variability of OB-type stars. *A&A*483(3):857–867. <https://doi.org/10.1051/0004-6361/20077740>, <https://arxiv.org/abs/arXiv:1008.4260> [astro-ph.SR]
- Schöller M, Hubrig S, Fossati L, et al (2017) B fields in OB stars (BOB): Concluding the FORS 2 observing campaign. *A&A*599:A66. <https://doi.org/10.1051/0004-6361/201628905>, <https://arxiv.org/abs/arXiv:1611.04502> [astro-ph.SR]
- Scowen PA, Gayley K, Neiner C, et al (2021) The Polstar High Resolution Spectropolarimetry MIDEX Mission. In: Society of Photo-Optical Instrumentation Engineers (SPIE) Conference Series, p 1181908, <https://doi.org/10.1117/12.2594267>, 2108.10729
- Shultz M, Wade GA (2017) Confirming the oblique rotator model for the extremely slowly rotating O8f?p star HD 108. *MNRAS*468(4):3985–3992. <https://doi.org/10.1093/mnras/stx759>, <https://arxiv.org/abs/arXiv:1703.08996> [astro-ph.SR]
- Shultz M, Wade GA, Rivinius T, et al (2017) The pulsating magnetosphere of the extremely slowly rotating magnetic β Cep star ξ^1 CMa. *MNRAS*471:2286–2310. <https://doi.org/10.1093/mnras/stx1632>, <https://arxiv.org/abs/arXiv:1706.08820> [astro-ph.SR]
- Shultz ME, Wade GA, Rivinius T, et al (2018) The magnetic early B-type stars I: magnetometry and rotation. *MNRAS*475:5144–5178. <https://doi.org/10.1093/mnras/sty103>, <https://arxiv.org/abs/arXiv:1801.02924> [astro-ph.SR]
- Shultz ME, Wade GA, Rivinius T, et al (2019) The magnetic early B-type stars - III. A main-sequence magnetic, rotational, and magnetospheric biography. *MNRAS*490(1):274–295. <https://doi.org/10.1093/mnras/stz2551>, <https://arxiv.org/abs/arXiv:1909.02530> [astro-ph.SR]
- Shultz ME, Owocki S, Rivinius T, et al (2020) The magnetic early B-type stars - IV. Breakout or leakage? H α emission as a diagnostic of plasma transport in centrifugal magnetospheres. *MNRAS*499(4):5379–5395. <https://doi.org/10.1093/mnras/staa3102>, <https://arxiv.org/abs/arXiv:2009.12336> [astro-ph.SR]
- Shultz ME, Owocki SP, ud-Doula A, et al (2022) MOBSTER – VI. The crucial influence of rotation on the radio magnetospheres of hot stars. arXiv e-prints arXiv:2201.05512. <https://arxiv.org/abs/arXiv:2201.05512> [astro-ph.SR]
- Sikora J, Wade GA, Power J, et al (2019) A volume-limited survey of mCP stars within 100 pc II: rotational and magnetic properties. *MNRAS*483(3):3127–3145. <https://doi.org/10.1093/mnras/sty2895>, <https://arxiv.org/abs/arXiv:1811.05635> [astro-ph.SR]
- Smith MA, Groote D (2001) Wind circulation in selected rotating magnetic early-B stars. *A&A*372:208–226. <https://doi.org/10.1051/0004-6361:20010472>, <https://arxiv.org/abs/arXiv:astro-ph/0104059> [astro-ph]
- Song HF, Meynet G, Maeder A, et al (2022) News from Gaia on σ Ori E: A case study for the wind magnetic braking process. *A&A*657:A60. <https://doi.org/10.1051/0004-6361/202141512>, <https://arxiv.org/abs/arXiv:2108.13734> [astro-ph.SR]
- St-Louis N, Gayley K, Hillier DJ, et al (2021) Ultraviolet Spectropolarimetry with

- Polstar: Massive Star Binary Colliding Winds. arXiv e-prints arXiv:2111.11552. <https://arxiv.org/abs/arXiv:2111.11552> [astro-ph.SR]
- Stahl O, Kaufer A, Rivinius T, et al (1996) Phase-locked photospheric and stellar-wind variations of θ^1 Orionis C. *A&A*312:539–548
- Takahashi K, Langer N (2021) Modeling of magneto-rotational stellar evolution. I. Method and first applications. *A&A*646:A19. <https://doi.org/10.1051/0004-6361/202039253>, <https://arxiv.org/abs/arXiv:2010.13909> [astro-ph.SR]
- Townsend RHD, Owocki SP (2005) A rigidly rotating magnetosphere model for circumstellar emission from magnetic OB stars. *MNRAS*357:251–264. <https://doi.org/10.1111/j.1365-2966.2005.08642.x>, <https://arxiv.org/abs/0408565>
- ud-Doula A (2008) Large-scale wind structure due to magnetic fields. In: Hamann WR, Feldmeier A, Oskinova LM (eds) *Clumping in Hot-Star Winds*, p 125
- ud-Doula A, Owocki SP (2002) Dynamical Simulations of Magnetically Channeled Line-driven Stellar Winds. I. Isothermal, Nonrotating, Radially Driven Flow. *ApJ*576(1):413–428. <https://doi.org/10.1086/341543>, <https://arxiv.org/abs/arXiv:astro-ph/0201195> [astro-ph]
- ud-Doula A, Owocki SP, Townsend RHD (2008) Dynamical simulations of magnetically channelled line-driven stellar winds - II. The effects of field-aligned rotation. *MNRAS*385(1):97–108. <https://doi.org/10.1111/j.1365-2966.2008.12840.x>, <https://arxiv.org/abs/arXiv:0712.2780> [astro-ph]
- ud-Doula A, Owocki SP, Townsend RHD (2009) Dynamical simulations of magnetically channelled line-driven stellar winds - III. Angular momentum loss and rotational spin-down. *MNRAS*392(3):1022–1033. <https://doi.org/10.1111/j.1365-2966.2008.14134.x>, <https://arxiv.org/abs/arXiv:0810.4247> [astro-ph]
- ud-Doula A, Cheung MCM, David-Uraz A, et al (2022) Ultraviolet Spectropolarimetric Diagnostics of Hot Star Magnetospheres. arXiv e-prints arXiv:2206.12838. <https://arxiv.org/abs/arXiv:2206.12838> [astro-ph.SR]
- Vink JS, de Koter A, Lamers HJGLM (2001) Mass-loss predictions for O and B stars as a function of metallicity. *A&A*369:574–588. <https://doi.org/10.1051/0004-6361:20010127>, <https://arxiv.org/abs/0101509>
- Wade GA, Neiner C, Alecian E, et al (2016) The MiMeS survey of magnetism in massive stars: introduction and overview. *MNRAS*456(1):2–22. <https://doi.org/10.1093/mnras/stv2568>, <https://arxiv.org/abs/arXiv:1511.08425> [astro-ph.SR]
- Wisniewski JP, Berdyugin AV, Berdyugina SV, et al (2021) UV Spectropolarimetry with Polstar: Protoplanetary Disks. arXiv e-prints arXiv:2111.06891. <https://arxiv.org/abs/arXiv:2111.06891> [astro-ph.IM]

Statements & Declarations

Funding

AuD acknowledges support by NASA through Chandra Award number TM1-22001B and GO2-23003X issued by the Chandra X-ray Observatory 27 Center, which is operated by the Smithsonian Astrophysical Observatory for and on behalf of NASA under contract NAS8-03060.

M.E.S. acknowledges financial support from the Annie Jump Cannon Fellowship, supported by the University of Delaware and endowed by the Mount Cuba Astronomical Observatory.

A.D.-U. is supported by NASA under award number 80GSFC21M0002.

C.E. gratefully acknowledges support for this work provided by NASA through grant number HST-AR-15794.001-A from the Space Telescope Science Institute, which is operated by AURA, Inc., under NASA contract NAS 5-26555. C.E. also gratefully acknowledges support from the National Science Foundation under Grant No. AST-2009412.

M.C.M.C. acknowledges internal research support from Lockheed Martin Advanced Technology Center.

This material is based upon work supported by the National Center for Atmospheric Research, which is a major facility sponsored by the National Science Foundation under Cooperative Agreement No. 1852977.

Y.N. acknowledges support from the Fonds National de la Recherche Scientifique (Belgium), the European Space Agency (ESA) and the Belgian Federal Science Policy Office (BELSPO) in the framework of the PRODEX Programme (contracts linked to XMM-Newton and Gaia).

N.S. acknowledges support provided by NAWA through grant number PPN/SZN/2020/1/00016/U/DRAFT/00001/U/00001.

G.A.W. acknowledges Discovery Grant support from the Natural Sciences and Engineering Research Council of Canada (NSERC).

Author Contributions

All authors contributed to the study conception and design. The first draft of the manuscript was written by M. E. Shultz and all authors commented on previous versions of the manuscript. All authors read and approved the final manuscript.

Data availability

The IUE data used to evaluate ultraviolet fluxes are available at the Mikulski Archive for Space Telescopes. The TLUSTY BSTAR2006 and OSTAR2002 libraries of synthetic spectra used to evaluate ultraviolet fluxes for stars without available IUE data are available online.

Competing Interests

The authors have no relevant financial or non-financial interests to disclose.

Affiliations

¹Department of Physics and Astronomy, University of Delaware, 217 Sharp Lab, Newark, Delaware, 19716, USA

²High Altitude Observatory, National Center for Atmospheric Research, P.O. Box 3000, Boulder CO 80307-3000, USA

³Lockheed Martin Solar and Astrophysics Laboratory, 3251 Hanover St, Palo Alto, CA 94304, USA

⁴Department of Physics and Astronomy, Howard University, Washington, DC 20059, USA

⁵Center for Research and Exploration in Space Science and Technology, and X-ray Astrophysics Laboratory, NASA/GSFC, Greenbelt, MD 20771, USA

⁶Instituto de Astrofísica de Canarias, E-38205 La Laguna, Tenerife, Spain

⁷Departamento de Astrofísica, Universidad de La Laguna, E-38206 La Laguna, Tenerife, Spain

⁸Department of Physics & Astronomy, East Tennessee State University, Johnson City, TN 37614, USA

⁹Tartu Observatory, University of Tartu, Observatooriumi 1, Tõravere, 61602, Estonia

¹⁰Department of Physics & Astronomy, University of Iowa, 203 Van Allen Hall, Iowa City, IA, 52242, USA

¹¹Anton Pannekoek Institute for Astronomy, University of Amsterdam, Science Park 904, 1098 XH, Amsterdam, The Netherlands

¹²Department of Physics and Astronomy, Uppsala University, Box 516, 75120 Uppsala, Sweden

¹³FNRS, Université de Liège, Allée du 6 Août 19c (B5C), B-4000 Sart Tilman, Liège, Belgium

¹⁴LESIA, Paris Observatory, PSL University, CNRS, Sorbonne Université, Univ. Paris Diderot, Sorbonne Paris Cité, 5 place Jules Janssen, 92195 Meudon, France

¹⁵Department of Physics, California Lutheran University, 60 West Olsen Road 3700, Thousand Oaks, CA, 91360, USA

¹⁶NASA Goddard Space Flight Center, 8800 Greenbelt Rd., Greenbelt, MD 20771

¹⁷Nicolaus Copernicus Astronomical Centre of the Polish Academy of Sciences, Bartycka 18, 00-716 Warsaw, Poland

¹⁸Penn State Scranton, 120 Ridge View Drive, Dunmore, PA 18512, US

¹⁹Armagh Observatory and Planetarium, College Hill, BT61 9DG Armagh, Northern Ireland

²⁰Department of Physics and Space Science, Royal Military College of Canada, PO Box 17000, Station Forces, Kingston, ON, K7K 7B4

²¹Department of Physics, Engineering Physics and Astronomy, Queen's University, Kingston, ON, Canada, K7L 3N6